Korean J. Chem. Eng., 34(4), 1208-1213 (2017)
DOI: 10.1007/s11814-016-0347-4

pISSN: 0256-1115
eISSN: 1975-7220

Effect of post-synthesis annealing on properties of SnS nanospheres and its solar cell performance

Nguyen Tam Nguyen Truong*, Ha Hai Thi Hoang*, Thanh Kieu Trinh*, Viet Thanh Hau Pham*, Ryan Patrick Smith, and Chinho Park*,†**

*School of Chemical Engineering, Yeungnam University, 280 Daehak-Ro, Gyeongsan 38541, Korea
**Department of Physics, California State University - East Bay, Hayward, CA 94542, U.S.A.
(*Received 24 August 2016 • accepted 10 December 2016*)

Abstract−SnS nanospheres (NSPs) were synthesized, and the effects of thermal annealing on the structural, morphological, chemical compositional and optical properties were examined. As-synthesized SnS NPSs with a mean size of 3-4 nm underwent a solid state morphological transformation by high temperature annealing in a nitrogen environment. Upon annealing, the size of SnS NSP increased to 5-6 nm with enhanced crystallinity. Also, the photoluminescence (PL) of the nitrogen-annealed samples slightly decreased in intensity with accompanying red-shift in spectrum. The power conversion efficiency of the solar cells using a polymer and the SnS NSPs was ~0.71%. These results confirm that the SnS NSPs demonstrate a potential as an inorganic material to be used in organic-inorganic hybrid bulk heterojunction (BHJ) photovoltaic devices.

Keywords: Tin Sulfide, Nanocrystal, Photoactive Layer, Orthorhombic, Bulk Hetero-Junction, Exciton

INTRODUCTION

Nanometer-sized inorganic semiconductors (PbS, PbTe, CdSe, InGa, SnTe, etc.) have attracted considerable attention as candidates for next-generation materials for energy devices. Many of the previously studied nanostructures, however, include either earth non-abundant or toxic elements such as Cd, Pb and In. Thus, there have been some doubts regarding whether these materials will contribute significantly to the future new and renewable energy supply. For this reason, high light-absorbing, non-toxic, abundant in nature, not posing any health or environmental hazards, and low-cost materials, such as CuS, SnS, and FeS_2, have recently attracted more interest as alternative materials for energy devices such as solar cells and secondary batteries [1-3]. SnS crystallizes in a strongly distorted NaCl structure (each Sn atom is coordinated by six S atoms), having orthorhombic geometry [4]. SnS has indirect and direct band gap of ~1.1 and ~1.3 eV, respectively [5,6], which is very close to the ideal value required for the strongest sunlight absorption. Due to this large sunlight-absorption coefficient [7] and tunable band gap by size-controlled quantum confinement property, SnS can be potentially useful as an absorber material in thin film photovoltaics [8], near-infrared detectors and other optoelectronic devices [9,10].

SnS nanoparticles (NPs) with different morphologies such as nanowires [11], fullerene-like nanoballs [12], nanobelts [13] have been synthesized using a range of methods, including spray pyrolytic deposition, plasma-enhanced chemical vapor deposition (CVD) and atmosphere pressure CVD [14-16]. Oda et al. [17] obtained colloidal SnS nanoparticles via wet chemical synthesis method with a controllable size by changing the synthesis temperature. Smaller nanoparticles showed more prominent quantum confinement effect with its band gap becoming larger, leading to a blue-shift in the sunlight absorption spectrum. The structural, morphological, and optical properties of SnS NPs have been previously studied, and characterization has been performed using AFM for morphology, TEM for size and XRD for structure identification [18].

However, the details of thermal annealing effects on the properties of SnS nanoparticles have not been reported. In this study, SnS nanospheres (NSPs) were synthesized, and the effects of a post-synthesis thermal treatment on the optical, morphological and chemical compositional properties of the NSPs were investigated. Bulk hetero-junction (BHJ) solar cells with the structure of indium tin oxide (ITO)/(PEDOT : PSS)/(SnS : polymer)/Al were fabricated by blending the nanoparticles with a conjugated polymer to form the active layer for the first time. Current density-voltage characterization of the devices showed that due to the addition of SnS nanoparticles to the polymer film, the device performance could be dramatically improved, compared with that of the pristine polymer solar cells.

EXPERIMENTAL

SnS NSPs were obtained by using a typical wet chemical synthesis method [17]. As-synthesized colloidal SnS nanoparticles were washed four times with hexane to remove the excess organic ligands and vacuum-dried to obtain the SnS NSPs. The NSPs were annealed at 350 °C for 30 min under a nitrogen environment using a hot-plate located in an N_2 glove box. The effects of thermal treatment in the nitrogen environment on the nanoparticle properties were then investigated.

†To whom correspondence should be addressed.
E-mail: chpark@ynu.ac.kr

The BHJ solar cells were then fabricated as follows: ITO-coated glass/PEDOT : PSS/(SnS+Polymer)/Al was then fabricated. A thin (~70 nm) layer of poly(ethylenedioxythiophene) doped with poly (styrene sulfonic acid)(PEDOT : PSS; Sigma Aldrich) was spin-coated at 4,000 rpm for 30 s onto cleaned indium tin oxide (ITO)-coated glass substrates, and dried at 100 °C for 30 min. The blend of SnS nanospheres and polymer (weight ratio 1 : 1, loading amount of 10 mg/mL) was dropped and spin-coated onto the preformed PEDOT : PSS layers at 4,000 rpm for 30 s to form the photoactive SnS/polymer bulk hetero-junction layers. The samples were then dried at 140 °C for 30 min under nitrogen flux in a glove box. Finally, a 100-nm-thick aluminum (Al) electrode was deposited on top of the film by thermal evaporation to complete the device structure. These polymers were used in this study such as poly(3-hexylthiophene-2,5-diyl)(P3HT), poly[2,6-(4,4-bis-(2-ethylhexyl)-4H-cyclopenta[2,1-b;3,4-b′]dithiophene)-alt-4,7(2,1,3-benzothiadiazole)] (PCPDTBT)), and (poly({4,8-bis[(2-ethylhexyl)oxy]benzo[1,2-b:4,5-b′]dithiophene-2,6-diyl}{3-fluoro-2-[(2 ethylhexyl)carbonyl] thieno [3,4-b]thiophenediyl}) (PTB7). The current density-voltage (J-V) characteristics of the devices were examined both in dark and AM1.5G illumination conditions using a solar simulator (Keithley 69911).

Optical properties of the NSPs were characterized by photoluminescence (PL) analysis. The morphology and particle size of the SnS NSPs were identified by atomic force microscopy (AFM), transmission electron microscopy (TEM) and high resolution-TEM (HR-TEM, H-7600 images). The chemical composition of the SnS NSPs was examined by X-ray photoelectron spectroscopy (XPS).

RESULTS AND DISCUSSION

Fig. 1 shows TEM images of SnS NSPs (a) as-synthesized and (b) nitrogen (N_2)-annealed at 350 °C for 30 min. As shown in Fig. 1(a), the as-synthesized NSPs had a mean diameter of ~3.9 nm (between ~3-4.5 nm) as calculated from a size distribution histogram (Fig. 1(a) inset). The synthesized NSPs were monodispersed and clearly separated without significant agglomeration. The N_2-annealed SnS NSPs at 350 °C for 30 min (Fig. 1(b)) retained the sharp morphology of the nanoparticle, but the size of the nanoparticles increased to a mean diameter of ~5.4 nm (between ~5-6 nm) as can be seen in Fig. 1(b) inset.

The HR-TEM images of the as-synthesized (Fig. 1(c)) and nitrogen-annealed (Fig. 1(d)) SnS NSPs showed well-resolved lattice fringes. The lattice fringe spacing of the as-synthesized and nitrogen-annealed SnS NPs were 0.32 and 0.54 nm, respectively, which are consistent with the distance between (021) planes of orthorhombic SnS [19], the as-synthesized and nitrogen-annealed at 350 °C samples both showed good crystallinity. Moreover, the lattice fringes were clearly visible, and there were no dislocations observed inside the nanospheres, confirming that the NSPs synthesized in this study were a single phase with very high quality. The morphology of SnS NSPs was examined further by observing the surface morphology of SnS film by AFM. A suspension of SnS NSPs in chloroform was prepared and stirred for 1 h before being deposited on a cleaned glass substrate (1×1 cm^2) by spin-coating, and the thin film coated substrates were dried at 80 °C in a drying oven. Fig.

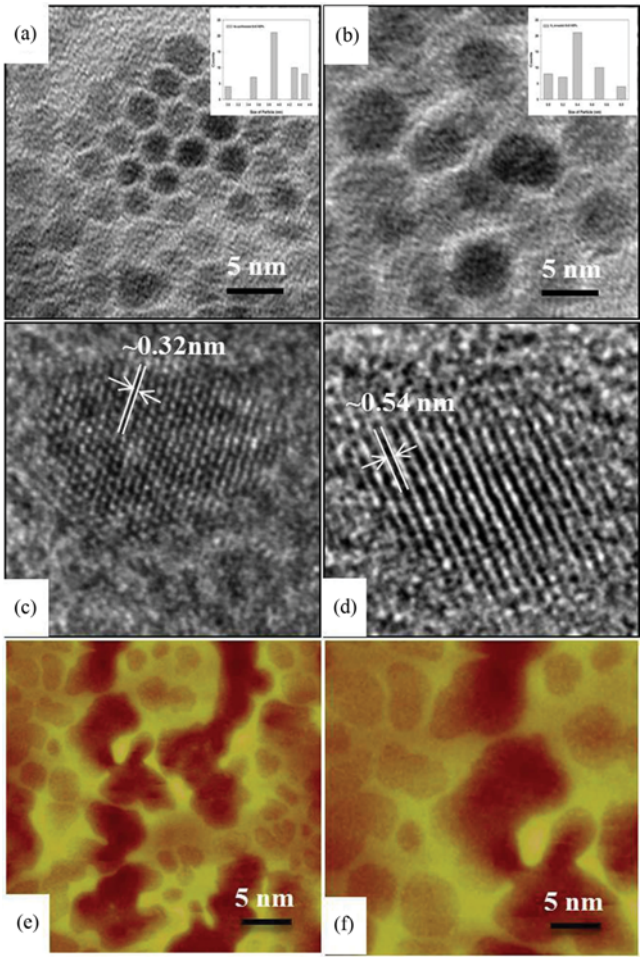

Fig. 1. TEM of SnS nanospherical: (a) As-synthesized; (b) nitrogen-annealed at 350 °C; HRTEM images of SnS nanospherical: (c) as-synthesized; (d) nitrogen-annealed at 350 °C.

1(e) and (f) show AFM images of the layers coated by as-synthesized and nitrogen-annealed SnS NSPs, respectively. The sizes of the as-synthesized and nitrogen-annealed SnS NPs were ~4.1 nm and 5.6 nm, respectively, which is consistent with the TEM results. This also shows that thermal annealing improves the crystallinity and increases the size of the SnS NSPs. The effects of thermal annealing on the nanocrystal's morphological properties such as size, shape and lattice fringe spacing were reported by many groups [20]. Researchers reported that an increase in the size of the annealed-SiO_2 nanoparticles was caused by the thermal diffusion-induced growth of the crystalline grains. The diffusion-induced bonding of smaller grains reduced the surface energy of the samples by reducing the free surface; the resulting larger grains in turn decreased the grain boundary area.

The effects of thermal annealing on the optical properties of SnS NSPs were investigated by photoluminescence analysis. Fig. 2 shows the room temperature PL spectra of the as-synthesized and nitrogen-annealed SnS NSPs. The as-synthesized SnS NSPs showed a clear PL emission peak at 916 nm (1.353 eV), which was blue-shifted by 37 nm (0.053 eV) from that of the bulk SnS (953 nm; 1.3 eV) [4,5]. The blue-shift in photoluminescence emission could be eas-

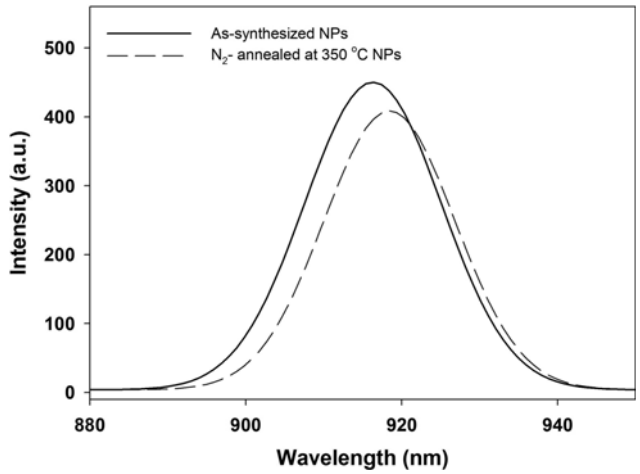

Fig. 2. PL spectrum of SnS nanospherical: (solid line) as-synthesized; (long dash line) nitrogen-annealed at 350 °C for 30 min.

ily explained by the quantum size effect [21]. In the semiconductor nanoparticles, the band gap increases with decreasing size, which is attributed to the quantum confinement of the carriers. After nitrogen-annealing of the as-synthesized SnS NSPs at 350 °C for 30 min, the photoluminescence emission intensity decreased, and the PL emission peak showed a red-shift by 2 nm (0.003 eV).

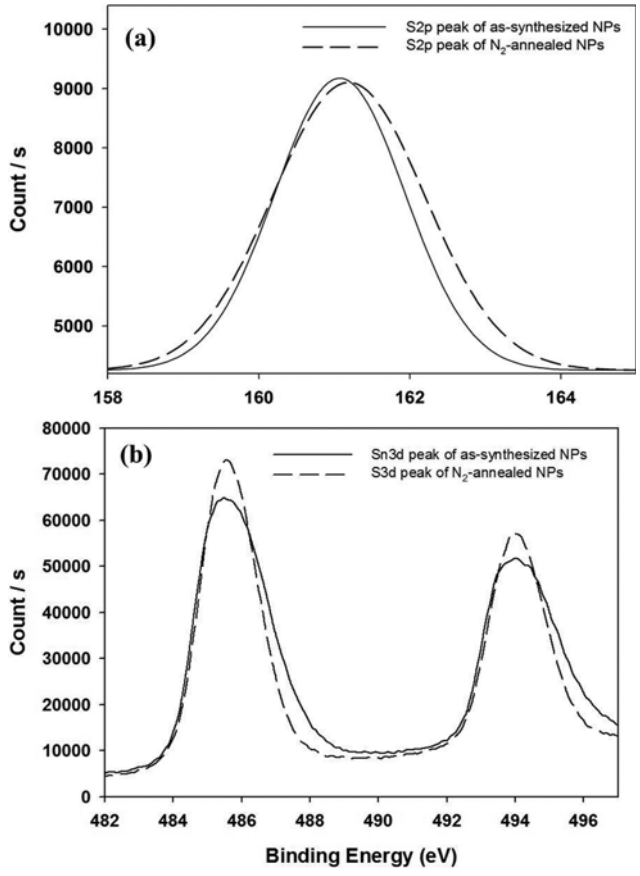

Fig. 3. XPS spectrum of as-synthesized and nitrogen annealed-SnS nanospherical: (a) S 2p spectrum, (b) Sn 3d spectrum.

Table 1. Binding energies of as-synthesized and nitrogen-annealed SnS NSPs measured from the corresponding Sn 3d and S 2p spectra (unit: eV)

Sample	S 2p	Sn $3d_{5/2}$	Sn $3d_{3/2}$
As-synthesized SnS NSPs	161.55	486.11	494.08
N_2-annealed SnS NSPs	161.91	486.19	494.16

The effects of thermal annealing on the optical properties of nanoparticle, especially the emission peak have been well studied and reported elsewhere. Alivisatos et al. [22] reported that the PL emission peak for cadmium selenide (CdSe) nanoparticles after annealing was red-shifted and the intensity of emission increased. The authors attributed these effects to oxygen which reacted with CdSe nanoparticles with possible formation of surface SeO_2 and CdO, influencing the PL enhancement. The optical properties of semiconductor nanoparticles are related to both extrinsic and intrinsic effects [23,24]. The PL data elucidated the crystalline quality and the purity in materials as well as exciton fine structure. A red-shift and intensity reduction of PL with increasing temperature can be induced by enhanced non-radiative recombination, and by temperature-dependent variations in the band structure. In our study, the red-shift and slight decrease in PL intensity suggest a reduction of point defects in the SnS nanoparticle after thermal treatment.

The effects of nitrogen annealing on the chemical bonding of SnS NSPs were examined by XPS (Fig. 3). The high resolution XPS spectra of the as-synthesized and N_2-annealed SnS NSPs were also recorded to reveal the detailed nature of the peaks. Table 1 lists the binding energies of the as-synthesized and N_2-annealed SnS NSPs, and Fig. 3(a) and 3(b) show the corresponding S 2p and Sn 3d peaks. The S 2p peak (Fig. 3(a)) of the N_2-annealed SnS NSPs shifted to a higher binding energy of 161.91 eV compared to that of the as-synthesized SnS NSPs (161.55 eV). The Sn 3d spectrum of as-synthesized SnS NSPs (as shown in Fig. 3(b)) revealed two peaks with binding energies of 486.11 eV and 494.08 eV, respectively, which is consistent with the 3d5/2 and 3d3/2 spin-orbit components. The high resolution XPS peaks were in good agreement with the data reported for SnS [25,26]. After annealing, the binding energy shifted to a higher value by approximately 0.08 eV, and the intensity of the Sn 3d levels increased, indicating the formation of stronger bonding within the SnS NSPs. The HR-XPS data shown in this study confirmed the absence of tin oxides, hydroxides and sulfur oxides, indicating that high-purity SnS NSPs were obtained after annealing in a nitrogen environment. From the aforementioned evidence, it is clear that the structural and optoelectronic properties of SnS NSPs were improved by nitrogen-annealing treatment at an elevated temperature. The effects of SnS NSPs thermal treatment on the performance of solar cells fabrication were also studied.

The devices were fabricated using a blend of P3HT as the electron donor and SnS NSPs (as-synthesized and nitrogen-annealed) as the electron acceptor (weight ratio 1 : 1, composite solution loading amount of 10 mg/mL) in the mixture solvent of chlorobenzene/chloroform (volume ratio 1 : 1). Fig. 4 shows the device's structure and device's characteristics with the structure of ITO-coated glass (ITO thickness of ~180 nm)/PEDOT : PSS (~70 nm)/(SnS+ P3HT) (~150 nm)/Al (~100 nm). The efficiency of the cells made

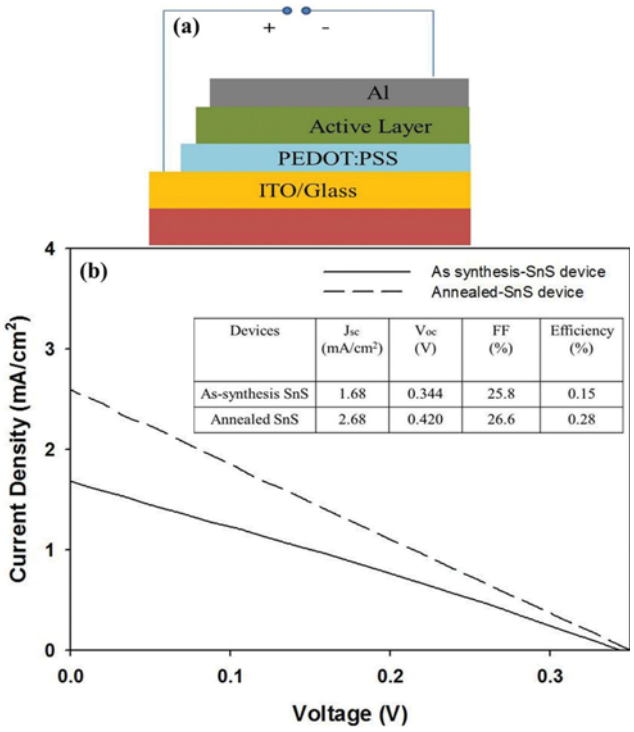

Devices	Jsc (mA/cm²)	Voc (V)	FF (%)	Efficiency (%)
As-synthesis SnS	1.68	0.344	25.8	0.15
Annealed SnS	2.68	0.420	26.6	0.28

Fig. 4. (a) Structure of the BHJ solar cells and (b) J-V curves of solar cells with structure of glass/ITO/PEDOT : PSS/(SnS+P3HT)/ Al (as-synthesis- and N_2 annealed-SnS).

from as-synthesized SnS NSPs was ~0.15% (Jsc: 1.68 mA/cm^2; Voc: 0.34 V), whereas the device made of nitrogen-annealed SnS NSPs showed an efficiency of ~0.28% (Jsc: 2.68 mA/cm^2; Voc: 0.42 V). Device made of nitrogen-annealed SnS NSPs showed an improvement in the efficiency of ~0.13%.

Results showed that due to the addition of SnS nanoparticles to the polymer film, the device performance can be dramatically improved, compared with that of the pristine polymer solar cells ~0.014% (Jsc: 2.01 mA/cm^2; Voc: 0.02 V).

Effects of the composite solution's loading amount on the device performance were also investigated. The device made of nitrogen-annealed SnS NPs showed a maximum efficiency of ~0.41% (Jsc: ~2.49 mA/cm^2) at the loading amount of 30 mg/mL. The device's efficiency in this study was still relatively low compared to that of the highest efficiency BHJ solar cells made from the nanocrystals and P3HT polymers, possibly due to the poorer charge collection because of poorer interfacial integrity between the polymer and SnS NSPs, poorer light harvesting, and roughness of the active layer surface morphology.

Fig. 5 shows that (a), (c) are the topography and (b), (d) are the 3-dimension (3D) AFM images of the active layer surface morphology. The root mean squared (RMS) surface roughness of as-synthesis SnS NSPs cells was ~15 nm, whereas the (RMS) surface roughness of nitrogen-annealed SnS NSPs cells was ~9 nm. The effects of photoactive layer's surface morphology on the exciton harvesting efficiency were reported elsewhere. The singlet excitons

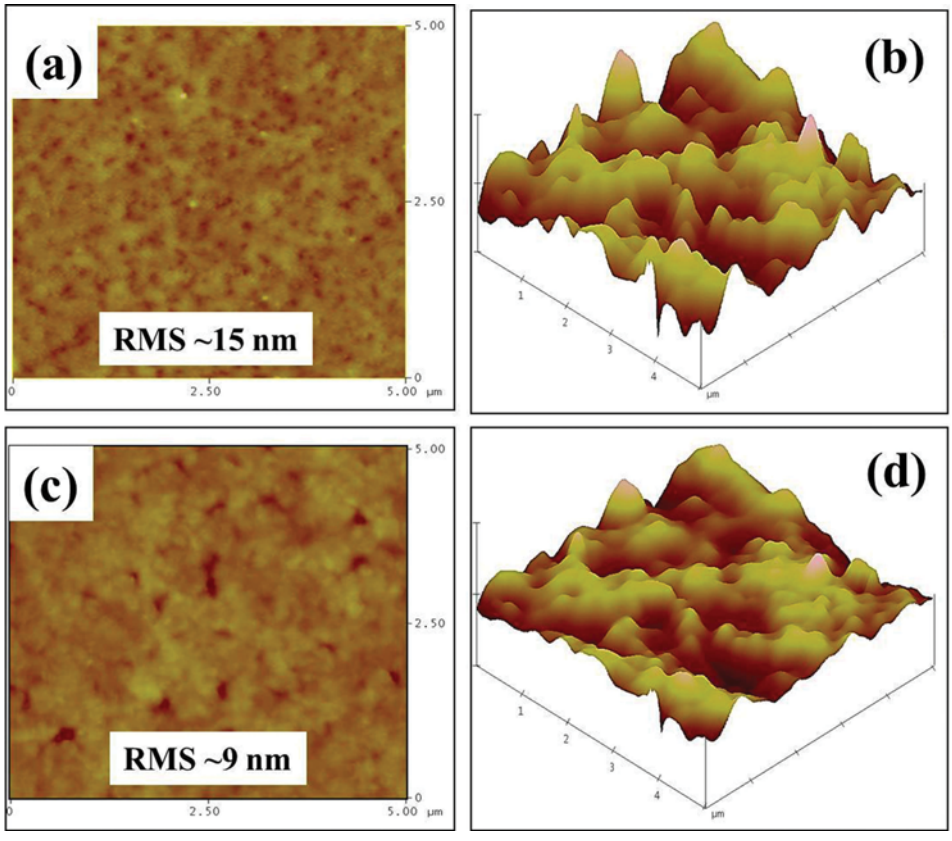

Fig. 5. (a), (b) Topography and 3-dimension-AFM image of (as-synthesis-SnS+P3HT) film and (c), (d) topography and 3-dimension image of (N_2-annealed-SnS+P3HT) film.

in organic materials are Coulombically bound electron-hole pairs, and hence cannot generate a photocurrent. For solar cell application, photoactive hetero-junction layers are used to generate charge carriers, at which excitons can be dissociated owing to the energy offset in the lowest unoccupied molecular orbital (LUMO) between n-type and p-type materials that is enough energy to break the Coulomb attraction [27]. So, excitons need to diffuse in to the p-n junction interface to convert to charge carriers before deactivating to the ground state. The exciton diffusion length (L_D) is a characteristic physical quantity, which is calculated by $L_D=(D\tau)1/2$, where D is the diffusion coefficient and τ is the exciton lifetime. Since the lifetime of singlet exciton in most conducting polymer films is short (<1 ns), the DL is limited to less than 20 nm for organic solar cells and 10 nm for inorganic solar cells. The DL is much shorter than the optical absorption pass length (~100-200 nm). So, only a limited part of the exciton can diffuse to the interface in photoactive layer hetero-junction solar cells. When the surface roughness of photoactive layer is smaller than the diffusion length, excitons can easily arrive at the interface, leading to enhanced exciton harvesting at the interface. However, if the surface roughness of photoactive layer is too small, charge collection is interrupted because of severe charge recombination [28]. This suggests that the SnS NCs and P3HT were dispersed nonuniformly in the photoactive layer, indicating that the surface roughness of the photoactive layer should be further optimized. Our measured efficiencies were slightly lower than those reported previously with a mixture of inorganic nanocrystals and P3HT with efficiencies that can approach ~1% with an optimization of the photoactive layer morphology, mixing ratio, thermal annealing, and film thickness [29,30].

The absorption spectra of P3HT cover the entire absorption band at 545-645 nm (as shown in Fig. 6 (inset) (solid-line)), with a band gap of ~1.9 eV. Therefore, the polymers which have longer absorption wavelength (low band gap energy) were designed to increase the harvesting of the solar spectrum. Fig. 6 (inset) (dot- and dash-line) shows the absorption wavelength of the (PCPDTBT)) and (PTB7) polymers, which covers the range of 350-900 nm.

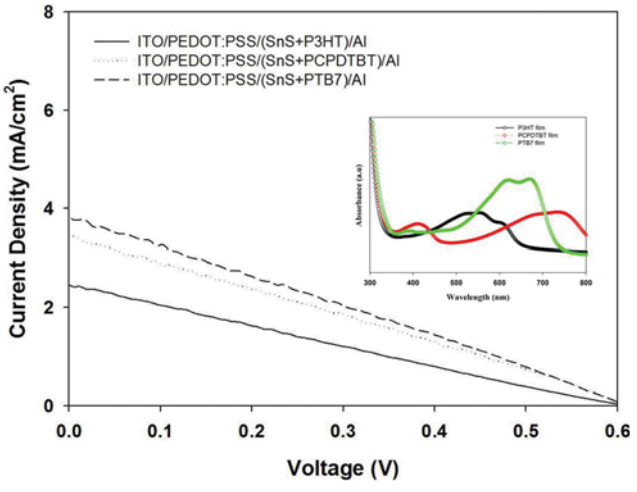

Fig. 6. (inset) Absorption spectra of pristine polymers such as P3HT, PCPDTBT, and PTB7 films and J-V curves of N_2-annealed-SnS based solar cells with different polymers.

Fig. 6 shows the J-V curves of the SnS/polymer devices, and the efficiency of the devices was found to be enhanced about double from ~0.41% (J_{sc}: ~2.49 mA/cm^2) of (SnS/P3HT cell) to ~0.55% (J_{sc}: ~3.43 mA/cm^2) of (SnS/PCPDTBT cell), and to ~0.71% (J_{sc}: ~3.90 mA/cm^2) of (SnS/PTB7 cell). The increased efficiency was mainly from the increase of the short-circuit current, which indicates an improvement in the light harvesting by PCPDTBT and PTB7 polymer because its absorption spectrum is extended to longer wavelength into the visible region.

Although the device parameters require further optimization to achieve commercial feasibility, solar cells devices using SnS NCs can be an alternative for cheap performance, simple, and environment-friendly polymer/inorganic hybrid solar cells, exhibiting long wavelength absorption up to 900 nm and desirable charge transport properties. Higher quality of nanospheres leads to enhanced interpenetration percolation pathways in photoactive layer morphology. Thus, it is concluded that the post synthesis annealing under nitrogen environment is a good way to improve the performance of inorganic-polymer bulk hetero-junction solar cells.

CONCLUSIONS

SnS nanospheres, 3-4 nm in size, were synthesized and characterized. High temperature nitrogen-annealing resulted in improved crystallinity of the nanospheres, an increase in the particle size and a decrease in the number of point defects. The as-synthesized SnS NSPs (mean size ~3-4 nm) showed a PL emission peak at 916 nm (1.353 eV), while the high temperature nitrogen-annealed SnS NSPs (average size ~5-6 nm) showed a PL emission peak at 918 nm (1.35 eV), which is closer to the bulk value (~1.3 eV). After annealing, the binding energy was shifted to a higher energy, indicating the formation of stronger atomic bonding within the SnS NSPs. The power conversion efficiency of the BHJ solar cells with a glass/ITO/PEDOT:PSS/(SnS+PTB7)/Al structure was ~0.71%, showing potential for SnS NSPs as an economic, earth-abundant and environment-friendly electron acceptor for the BHJ solar cells.

ACKNOWLEDGEMENTS

This work was supported by the New & Renewable Energy Core Technology Program (No. 20133030011330) and the Human Resources Program in Energy Technology (No. 20154030200760) of the Korea Institute of Energy Technology Evaluation and Planning (KETEP) granted financial resource from the Ministry of Trade, Industry & Energy, Republic of Korea.

REFERENCES

1. E. Hong, T. Choi and J. H. Kim, *Korean J. Chem. Eng.*, **32**, 424 (2015).
2. H. Peng, L. Jiang, J. Huang and G. Li, *J. Nanopart. Res.*, **9**, 1163 (2007).
3. N. T. N. Truong, T. P. N. Nguyen and C. Park, *Inter. J. Photoenergy*, **2013**, ID 146582 (2013).
4. L . Burton and A. Wash, *J. Phys. Chem.* C., **116**, 24262 (2012).
5. K. T. R. Reddy, N. K. Reddy and R. W. Miles, *Sol. Energy Mater.*

Sol. Cells, **90**, 3041 (2006).
6. M. Sugiyama, Y. Murata, T. Shimizu, K. Ramya, C. Venkataiah, T. Sato and K. T. R. Reddy, *Jpn. J. Appl. Phys.*, **50**, 05FH03 (2011).
7. G. H. Yue, D. L. Peng, P. X. Yan, L. S. Wang, W. Wang and X. H. Luo, *J. Alloys. Compd.*, **468**, 254 (2009).
8. K. T. R. Reddy, P. Reddy, P. K. Datta and R. W. Miles, *Thin Solid Films*, **403**, 116 (2002).
9. N. K. Reddy, Y. B. Hahn, Y. B. Devika, H. R. Sumana and K. R. Gunasekhar, *J. Appl. Phys.*, **101**, 093522 (2007).
10. P. Pramanik, P. K. Basu and S. Biswas, *Thin Solid Films*, **150**, 269 (1987).
11. C. An, K. Tang, Y. Jin, Q. Liu, X. Chen and Y. Qian, *J. Cryst. Growth*, **252**, 575 (2003).
12. S. Y. Hong, R. P. Biro, Y. Prior and R. Tenne, *J. Am. Chem. Soc.*, **125**, 10470 (2003).
13. J. Liu and D. Xue, *Electrochimica Acta*, **56**, 243 (2010).
14. B. Thangaraju and P. Kaliannan, *J. Phys. D: Appl. Phys.*, **33**, 1054 (2000).
15. A. Ortiz, J. C. Alonso, M. Garcia and J. Toriz, *Semicond. Sci. Technol.*, **11**, 243 (1996).
16. L. S. Price, U. P. Parkin, A. M. E. Hardy, R. J. H. Clark, T. G. Hibbert and K. C. Molloy, *Chem. Mater.*, **11**, 1792 (1999).
17. Y. Oda, H. Shen, L. Zhao, J. Li, M. Iwamoto and H. Lin, *Sci. Technol. Adv. Mater.*, **15**, 035006 (2014).
18. S. Sohila, M. Rajalakshmi, C. Chosh, A. K. Arora and C. Muthamizhchelvan, *J. Alloys Compound*, **509**, 5843 (2011).
19. S. Sohila, M. Rajalakshmi, C. Muthamizhchelvan, S. Kalavathi, C. Ghosh, R. Divakar, C. N. Venkiteswaran, N. G. Muralidharan, A. K. Arora and E. Mohandas, *Mater. Lett.*, **65**, 1148 (2011).
20. R. S. Zeferino, U. Pal, R. Melendrez and M. B. Flores, *Adv. Nano Res.*, **1**, 193 (2013).
21. L. E. Brus, *J. Chem. Phys.*, **80**, 4403 (1984).
22. A. P. Alivisatos, *J. Phys. Chem.*, **100**, 13226 (1996).
23. Y. P. Varshni, *Physica.*, **34**, 149 (1967).
24. S. Luo, J. Fan, W. Liu, M. Zhang,Z. Song, C. Lin, X. Wu and P. K Chu, *Nanotechnology*, **17**, 1695 (2006).
25. L. S. Price, I. P. Parkin, M. N. Field, A. M. E. Hardy, R. J. H. Clark, T. G. Hibbert and K. C. Molloy, *J. Mater. Chem.*, **10**, 527 (2000).
26. Y. Zhao, Z. Zhang, H. Dang and W. Liu, *Mater. Sci. Eng. B.*, **113**, 175 (2004).
27. S. D. Baranovskii, M. Wiemer, A. V. Nenashev, F. Jansson and F. Gebhard, *J. Phys. Chem. Lett.*, **3**, 1214 (2012).
28. G. Yu, J. Gao, J. C. Hummelen, F. Wudl and A. J. Heeger, *Science*, **270**, 1789 (1995).
29. I. Lokteva, N. Radychev, F. Witt, H. Borchert, J. Parisi and J. K. Olesiak, *J. Phys. Chem.*, **114**, 12784 (2010).
30. P. E. Shaw, A. Ruseckas and I. D. Samuel, *Adv. Mater.*, **20**, 3516 (2008).